Magnetic Resonance Imaging xxx (2015) xxx–xxx

Contents lists available at ScienceDirect

Magnetic Resonance Imaging

journal homepage: www.mrijournal.com

Pancreatic cancer growth using magnetic resonance and bioluminescence imaging

Rossana Ritelli [a], Raphael Ngalani Ngaleu [b], Pietro Bontempi [c], Mario Dandrea [a], Elena Nicolato [b], Federico Boschi [d], Silvia Fiorini [b], Laura Calderan [b], Aldo Scarpa [a], Pasquina Marzola [d,*]

[a] Department of Pathology and Diagnostics, University of Verona, Piazzale A. Scuro 10-37134, Italy
[b] Department of Neurological and Movement Sciences, University of Verona, Piazzale A. Scuro 10-37134, Italy
[c] Department of Biotechnology, University of Verona, Strada Le Grazie 15, 37134 Verona, Italy
[d] Department of Computer Science, University of Verona, Strada Le Grazie 15, 37134 Verona, Italy

ARTICLE INFO

Article history:
Received 28 August 2014
Revised 19 January 2015
Accepted 16 February 2015
Available online xxxx

Keywords:
Pancreas
Tumor
MRI
Optical imaging

ABSTRACT

Object: Pancreatic cancer is one of the most lethal human cancer and appropriate experimental tumor models are needed for the development of innovative therapeutic approaches. This paper describes an experimental model of human pancreatic cancer and a related non invasive imaging technique suitable for monitoring tumor growth and metastatization. The aim of the work was the implementation of an experimental platform suitable for assessing the efficacy of new therapeutic agents.
Materials and methods: Human pancreatic cancer cells (PANC-1-Luc+) were injected into the pancreas of female athymic CD1 mice. Magnetic Resonance Imaging (MRI) at 4.7 T and Bioluminescence Imaging (BLI) were performed in each mouse at three time points after cell inoculation (1, 2 and 3 months). Two groups of mice were studied: the first group of n = 13 mice in which $5 * 10^6$ cells were injected and the second group of n = 10 mice in which $2 * 10^6$ cells were injected. MRI examination included T2w acquisitions and (at the last time point) Dynamic-contrast-enhanced-MRI (DCE-MRI).
Results: Each mouse underwent three longitudinal MRI and BLI examinations. BLI was more sensitive than MRI producing higher detection rate at early time points. Moreover in one case of abdominal dissemination of pancreatic tumor cells, small tumoral masses were detected by BLI and not detected by MRI. However BLI appears more prone to experimental error most likely due to photon attenuation. In 4 mice BLI produced false negative results. DCE-MRI experiments providing information on tumor perfusion were conducted successfully in this anatomical district and demonstrated that the tumor tissues from the second experimental group are more vascularized compared to the first group.
Conclusion: The present study performed on the experimental model of pancreatic cancer here described shows that MRI and BLI are complementary techniques and that synergistic application of both can overcome the intrinsic limitations of each.

1. Introduction

Pancreatic cancer is one of the most lethal human cancers with an overall survival rate of 3%–5% and a median survival of less than 6 months. The short median survival is explained by the absence of early symptoms and the lack of appropriate diagnostic tools for early detection. The cancer's lethal nature results from its propensity to rapidly disseminate to the lymphatic system and distant organs, which occurs in more than 80% of cases. Metastasis to loco-regional lymph nodes or distant organs is one of the major features of pancreatic cancer and is typically already present at the time of diagnosis. This aggressive biology and resistance to conventional and targeted therapeutic agents lead to a typical clinical presentation of incurable disease at the time of diagnosis, even nowadays. Despite great efforts in recent years, conventional treatment approaches have little impact on the course of this aggressive neoplasm [1]. Therefore, reproducible preclinical models are required to study the underlying causes of tumor development, and the growth and dissemination of pancreatic cancer. These models, as well as the development of diagnostic imaging techniques to monitor tumor growth and metastasis formation, would also be crucial for the development of new and effective treatment modalities.

* Corresponding author. Tel.: +39 0458027614; fax: +39 0458027613.
E-mail addresses: rossanaritelli@libero.it (R. Ritelli), ngalaningaleu.raphael@univr.it (R. Ngalani Ngaleu), pietro.bontempi@univr.it (P. Bontempi), mario.dandrea@univr.it (M. Dandrea), elena.nicolato@univr.it (E. Nicolato), federico.boschi@univr.it (F. Boschi), silvia.fiorini@univr.it (S. Fiorini), laura.calderan@univr.it (L. Calderan), aldo.scarpa@univr.it (A. Scarpa), pasquina.marzola@univr.it (P. Marzola).

http://dx.doi.org/10.1016/j.mri.2015.02.017
0730-725X/

Currently, several mouse models of pancreatic cancer have been established [2]. The use of animal models in preclinical and basic studies makes it possible to test diagnostic markers and drugs, producing data that are more predictive of the distribution and efficacy of a compound [3]. In recent years new technologies have become available for imaging small animals, and noninvasive imaging in animal models has assumed increasing importance in preclinical research, so that it is now an independent specialty [4,5]. These imaging modalities, which include Magnetic Resonance Imaging (MRI), Computed Tomography (CT), Positron-Emission Tomography (PET), Single Photon Emission Tomography (SPECT), Optical Imaging (OI) and Ultrasound (US), have been utilized to evaluate the pharmacologic activity of novel targeted therapies [6,7]. However, each of these imaging methods has distinct advantages and limitations, and there are marked differences between their detection sensitivity, spatial and temporal resolution. The use of multiple imaging methods is therefore likely to provide complementary information on tumor biology [6,7] and response to therapies. Recently Partecke et al. [5] have reported the application of MRI to monitor the development of an orthotopic pancreatic tumor model in mice. The present paper extends the approach developed by Partecke et al. by adding Bioluminescence Imaging (BLI) to the equation in order to further improve longitudinal assessment of tumor evolution/regression.

It has been previously demonstrated that it is possible to select Panc-1 sphere cells which are stem-like cells starting from Panc-1 adherent cell line [8]. Panc-1 sphere cells can mimic the stem-like cell population in pancreatic cancer, but Panc-1 adherent cells may be a more reliable model for preclinical applications [8].

In this study, an experimental model of orthotopic pancreatic cancer was implemented by orthotopic injection of Panc-1 adherent cells transfected with the gene reporter Luciferase (Luc). Tumor development was studied over time using non-invasive imaging techniques, namely Optical Imaging in the bioluminescence modality and Magnetic Resonance Imaging. Each technique showed advantages and disadvantages that will be discussed. The aim of this study was to define an experimental pancreatic tumor model and suitable imaging modalities, to serve as experimental platform for testing new therapeutic agents.

2. Materials and methods

2.1. Orthotopic human pancreatic xenografts in immunodeficient mice

Experiments were carried out in compliance with national regulations and were approved by the Ethics Committee of our Institution. Human pancreatic cancer cell lines Panc-1-Luc+, were kindly provided by Dr. Scott Kern (Departments of Surgery, Pathology, and Oncology, The Johns Hopkins Medical Institutions, Baltimore, MD, USA) and maintained under G418 selection. The transfection procedure has been previously described [9]. Bioluminescence activity of Panc-1-Luc + cells was tested before injection in vivo.

Mice (female athymic CD1 mice, 4 weeks old, Charles River, Lecco, Italy) were anesthetized using a ketamine/xylazine cocktail at a ratio of 100 mg kg^{-1}:20 mg kg^{-1}. The abdominal skin was raised with forceps and a 1-cm incision with sterile micro-scissors was made slightly medial to the splenic silhouette. A second 1-cm incision was extended into the abdominal cavity without injuring the underlying organs. Using a pair of blunt-nose forceps, the tip of the pancreatic tail was gently grasped and the pancreas/spleen was externalized in the lateral direction, exposing the entire pancreatic body and spleen. While gently retracting the pancreas laterally, a needle was inserted into the tail of the pancreas and passed into the pancreatic head region; cells, suspended in 60 μl of PBS containing 1% serum-free Matrigel (vol/vol), were slowly injected while withdrawing the needle to the mid-body of the pancreas, forming a fluid-filled region within the pancreatic parenchyma. Then the pancreas/spleen was internalized using blunt forceps and the abdominal muscle layer was closed with continuous suture, while the overlying skin was closed with a second set of interrupted suture.

The mice were divided into two groups: group n.1 included mice (n = 13) injected with $5 * 10^6$ Panc-1 Luc + cells, and group n.2 (n = 10) with $2 * 10^6$ Panc-1 Luc + cells. Each animal was imaged using BLI and MRI one, two and three months after cell injection. Prior to BLI acquisition, the scarring at the level of the pancreas was carefully examined in order to assess the completion of wound healing.

2.2. Optical images acquisition and analysis

All the acquisitions were performed using the IVIS 200 optical imager (PerkinElmer, Hopkinton, MA, USA), equipped with a −90 °C cooled camera sensor back-thinned, back-illuminated grade 1 CCD 2.7 × 2.7 cm, 2048 × 2048 pixels. The images were acquired in bioluminescence modality (without excitation lamps and without emission filters) using the following parameters: Exposure time = 300 s; Binning = 8; f/stop (diaphragm opening) = 1; field of view = 12.8 cm.

During luciferin injection and image acquisition, the mice were kept under gaseous anesthesia (2% of isoflurane and 1 l/min of oxygen) on the heated plate of the instrument. After a pre injection image, which was acquired in order to assess the background emission, luciferin was injected intraperitoneally (15 mg/mL in PBS, dose of 150 mg/kg, D-luciferin, Firefly, potassium salt, 1.0 g/vial, Caliper Life Sciences, Hopkinton, MA, USA). Then three post-injection images were acquired at 5, 10 and 15 min. Images were acquired and analyzed using Living Image 4.1 (PerkinElmer, Hopkinton, MA, USA). Measurements were done in two ways. In the first one, Regions of Interest (ROIs) were traced manually on the optical images in order to measure the photon emission escaping from the animals' skin in the abdominal location within the selected ROI. In the second one, a threshold in the light intensity was fixed for all the images and the area with signal greater than the threshold was measured.

2.3. MRI images acquisition and analysis

Mice were anesthetized by inhalation of a mixture of air and O_2 containing 0.5%–1% isoflurane and placed in prone position inside a 3.5 cm i.d. transmitter–receiver birdcage coil. Images were acquired using a Biospec Tomograph (Bruker, Karlsruhe, Germany) equipped with a 4.7 T, 33 cm bore horizontal magnet (Oxford Ltd., Oxford, United Kingdom). The imaging planes were coronal and transversal. T2-weighted images were acquired using a T2w RARE sequence with the following parameters. Coronal plane: TR = 4400 ms, TE_{eff} = 67.2 ms, Field of view = 5.30 × 5.30 cm^2, Matrix size = 256 × 256, slice thickness = 1 mm, interslice distance = 1 mm. Transversal plane: TR = 5000 ms, TEeff = 56 ms, Field of view: 5 × 2.5 cm^2, Matrix size: 256 × 128, slice thickness = 1 mm, interslice distance = 1 mm. The hyperintense region, relative to the surrounding tissues in the specific anatomical region, was considered as tumor. In each slice, the tumor region was manually delineated by using the Region-of-Interest function of the software ParaVision 5.1 (Bruker, Karlsruhe, Germany). Tumor volumes were quantified by multiplying the number of tumor voxels by the individual voxel size. In the last imaging session, Dynamic Contrast Enhancement (DCE-MRI) experiments were also executed. Briefly, T1w RARE images were acquired before and at different time points after i.v. injection of the contrast agent (Gd-DTPA, Magnevist, Schering, Germany) at a 100 μmol/kg dosage. The parameters used were: TR = 733 ms, TE_{eff} = 10.7 ms, FOV = 3 × 3cm^2, Matrix size = 256 × 128 zero filled at 256 × 256; slice thickness = 0.75 mm, number of slices = 12. According to

Please cite this article as: Ritelli R, et al, Pancreatic cancer growth using magnetic resonance and bioluminescence imaging, Magn Reson Imaging (2015), http://dx.doi.org/10.1016/j.mri.2015.02.017

previously published experimental protocols [10,11], a total of 22 images were acquired with a time resolution of 105 s. Three regions-of-Interest (ROIs) were manually drawn to quantify the signal in the external and internal part of the tumor and in the skeletal muscle. The external part of the tumor was considered as the strongly enhancing region at the tumor periphery and corresponded in most of tumors to a 2–3 mm wide band. The remaining area in the tumor slice was considered as belonging to the internal ROI. DCE-MRI data were quantified by calculating the Area-Under-the-Curve (AUC) of the time dependence of the Signal Intensity Enhancement for the first 10 min after contrast agent injection.

Both BLI and MRI images were independently analyzed by two researchers (PB and RR) for the presence of tumor signal. In discordant cases, a consensus reading was performed.

2.4. Ex vivo histological and immunohistochemical analysis of tumor xenografts

Three months after tumor induction, mice were sacrificed by cervical dislocation for necropsy and tumor excision. After excision, tumor masses were photographed and tumor diameters (d and D) were measured by caliber. The tumor volume was calculated according to the formula: $V = (d^2 \times D/2)$. Tumor samples were then formalin-fixed, embedded in paraffin, sectioned and de-paraffinized using xylene, and hydrated by series of decreasing ethanol washes. Hematoxylin/Eosin (H&E) staining was performed for each sample.

3. Results

3.1. Sensitivity of BLI and MRI

Magnetic Resonance and BLI Images were acquired one, two and three months after cell injection. Two researchers with experience in MRI of experimental tumors evaluated tumor detectability in MR images. The number of subjects in which tumors were detected is shown in Table 1. In the first group of mice ($5 * 10^6$cells) tumors were detected in each mouse at one, two and three months after injection using both MRI and BLI. At the first time point only twelve mice were imaged using BLI because of experimental problems. Moreover, at the third time point, data relative to only twelve mice are presented because one mouse was sacrificed two months after cell injection due to excessive tumor growth and intestinal invasion (see Fig. 3).

In the second group of mice ($2 * 10^6$cells) tumors were not detectable in a great number of animals, especially at the first time point. In this group, BLI detected more tumors than MRI at early time points, but with the increase in tumor size, MRI proved to be as sensitive as BLI. Moreover BLI detection of tumor was prone to experimental errors, because in $n = 4$ mice belonging to the second experimental group, tumors were detected at a given time point and not detected at the following time point (false negative). It is worthwhile to mention that false negative response is easily due to misinjection of luciferin into the intestinal tract rather than i.p. and by repeating the injection this issue could be eliminated.

Table 1
Sensitivity of OI and MRI techniques.

Experiment	1st month	2nd month	3rd month
MRI ($5 * 10^6$ cells)	13/13	13/13	12/12
OI ($5 * 10^6$ cells)	12/12	13/13	12/12
MRI ($2 * 10^6$ cells)	3/10	6/10	8/10
OI ($2 * 10^6$ cells)	5/10	7/10	8/10

Data are reported as the number of tumors detected over the number of subjects imaged.

3.2. Tumor growth

Representative BLI and MRI images acquired in a mouse belonging to experimental group n.1 are shown in Fig. 1. Fig. 1g and h shows the time evolution of average tumor size measured by MRI while Fig. 1i and j shows results obtained by BLI; data are reported as mean ± SEM. The MRI readout of tumor size is represented by tumor volume expressed in mm^3 while the BLI readout is represented by the light flux (number of photons/s). Both techniques showed that tumor size increased more rapidly in the first group than in the second one. In experimental group n.2, tumor volumes at MRI were about ten times smaller than in experimental group n.1 and, especially at the first time point, were determined with considerable uncertainty due to the small size of the tumors themselves and the confounding effect of abdominal structures. This contributed to the low detection rate of tumors in this experimental group.

In BLI data from animals belonging to experimental group n.2 we observed wide variability of tumor size (unlike MRI data from the same group). This variability was partly due to the smaller number of data available in this group, since some animals were excluded ($n = 4$) because no emission was detected.

In some mice (belonging mainly to experimental group n.2) we found a non-monotonic trend: photon flux measured two months after cell injection was higher than the value measured three months after. This finding is in contrast with the volume measured using MRI, which showed a monotonic increasing trend over time in each animal (see graphical insert in Fig. 1).

3.3. Correlation between MRI and BLI

We investigated the correlation between the MRI-determined tumor volume and BLI signal in the first group of animals ($5 * 10^6$ cells). Results are reported in Table 2 as correlation coefficients of the assumed linear relationship. There was a good linear correlation between MRI and BLI photon flux when correlating all time points. This correlation worsens when each time point is analyzed separately. At the first and second time point there is low or no correlation at all (data not shown), while at the third time point a good linear correlation was obtained.

Following Bouvet et al. [12], the correlation between the MRI volume and the BLI area was also analyzed. As shown in Table 2, the correlation between MRI and BLI data improved when BLI area is considered instead of photon flux. For the last time point (three months, Table 2 c, d) the correlation coefficient, R^2, was substantially higher when correlating BLI area vs. MRI volume than when correlating BLI flux vs. MRI volume. In the first case, analyzing all mice observed at the third time point alone, an R^2 value equal to 0.82 was obtained (Table 2c). The correlation between MRI/BLI readouts and the tumor volumes as determined by ex vivo measurements was then investigated. Results are shown in the last three columns of Table 2 and are obviously restricted to the last time point (c and d lines). A very good correlation was detected between ex vivo and MRI determined tumor volumes, while the correlation with BLI readouts was poor. Among the two considered BLI readouts, the BLI area was correlated to ex vivo tumor volumes better than photon flux.

In the second group of animals ($2 * 10^6$ cells) the correlation between MRI and BLI was substantially lower than in the first group, a correlation coefficient $R^2 = 0.51$ was obtained by including in the analysis all mice in which tumors were detected by both techniques at the different time points.

3.4. DCE-MRI

Dynamic Contrast Enhancement MRI (DCE-MRI) experiments were performed in both experimental groups at the last time point.

Please cite this article as: Ritelli R, et al, Pancreatic cancer growth using magnetic resonance and bioluminescence imaging, Magn Reson Imaging (2015), http://dx.doi.org/10.1016/j.mri.2015.02.017

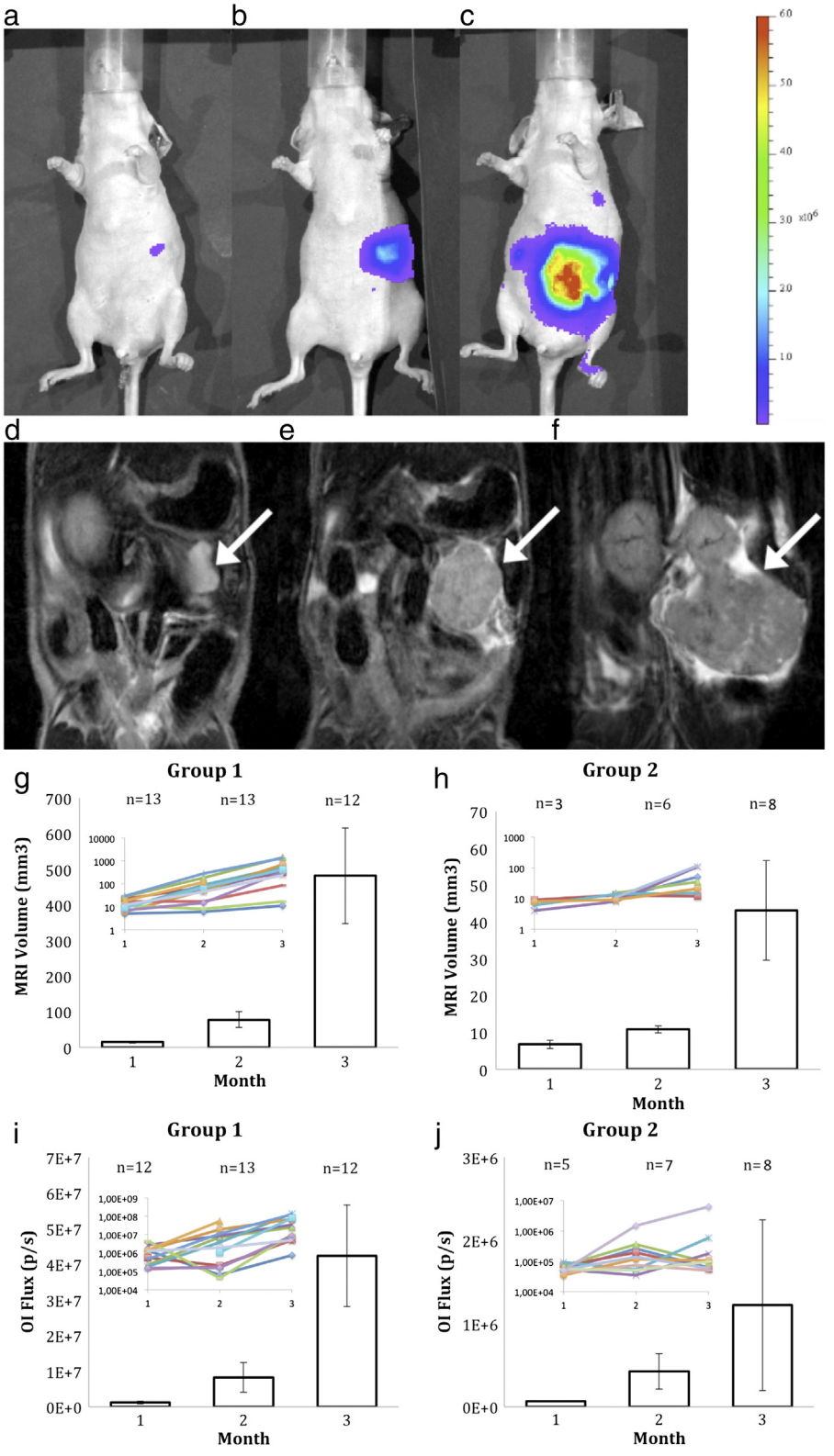

Fig. 1. BLI and MRI in the longitudinal investigation of tumor growth. Representative Bioluminescence (a, b and c) and MR (d, e and f) images acquired in a subject belonging to experimental group n.1 at 1, 2 and 3 months after cell injection. Color bar reports photon flux expressed as (number of photons)/s/cm^2/sr. The arrows in panels d–f indicate the tumor mass. Panels g, h, i and j show the time dependence of tumor size assessed using MRI and BLI in the two experimental groups. Panels g and i present data from the first group of animals as obtained with MRI and OI respectively. Panels h and j present data from the second group of animals. In the insert individual size data are shown on a logarithmic scale.

Please cite this article as: Ritelli R, et al, Pancreatic cancer growth using magnetic resonance and bioluminescence imaging, Magn Reson Imaging (2015), http://dx.doi.org/10.1016/j.mri.2015.02.017

Table 2
Correlation coefficient (R^2) among MRI, BLI and ex vivo determination of tumor volumes in the experimental group n.1.

R^2	MRI vol vs. photon fluxes	MRI vol vs. BLI areas	Ex vivo vol vs. MRI vol	Ex vivo vol vs. photon flux	Ex vivo vol vs BLI area
a	0.68	0.72	/	/	/
b	0.69	0.77	/	/	/
c	0.61	0.82	0.98	0.57	0.76
d	0.55	0.76	0.98	0.49	0.66

We considered 4 sub-groups of animals: a) all mice, all time points; b) only mice that showed a monotonic increasing trend of photon fluxes, all time points; c) all mice, third time point only; d) only those mice that featured a monotonic growth (third time point only). Photon Fluxes and BLI Areas are relative to quantitative values extracted from bioluminescence images. In the first case the photon flux in a selected ROI was measured. In the second case the area of the region in the image in which the photon flux was higher than a selected threshold was measured.

T1w images were acquired before and, dynamically, after injection of Gd-DTPA at the clinical dosage of 100 μmol/kg. Fig. 2 shows representative T1w, axial images acquired before (Fig. 2a) and immediately after injection of Gd-DTPA (Fig. 2b) in a mouse belonging to experimental group n.1. Fig. 2c shows positioning of ROIs used to evaluate AUC in the external and internal part of the tumor and in the skeletal muscle. Fig. 2d and e shows the time dependence of signal intensity (SI, normalized to the signal intensity before contrast agent injection) in the three Regions of Interest (ROIs), for representative animals belonging to the experimental group n.1 and n.2, respectively. In both groups, the time dependence of SI clearly discriminates between external and internal regions of the tumor. The time course of the signal intensity for group n.2 clearly shows faster response to contrast agent in the core of the tumor when compared to group n.1. Outer tumor and muscle show similar behavior with respect to group n.1. For both groups, in the external region, SI shows a faster and larger increase than in the internal ROI; this corresponds to the presence of highly vascularized tissue generally observed in the external part of xenografts in comparison to the internal part [10,11]. It is worthwhile to mention that the experimental observation of differential vascularization between internal and external region of the tumor, commonly observed also in other xenograft tumor models as for example colon carcinoma [10,11], does not mean that the present experimental model is highly vascularized as these other models are. The enhancement of the SI is in fact strongly dependent on several acquisition parameters, including acquisition sequence and its timing contrast agent and dosage field strength, which should be carefully checked in order to perform a similar comparison. DCE-MRI curves were quantitatively analyzed using the Area-Under-the-Curve (AUC) [10]. Two ROIs were included in the analysis: one ROI was manually drawn to cover all tumor tissue and a second ROI was placed over skeletal muscle. The AUC values (in the time interval 0–10 min after contrast agent injection) were calculated for both tumor and muscle tissues. In experimental group n.1, the average AUC (normalized to muscle) amounted to 1.92 ± 0.63 (mean $\pm$ SD), which was significantly lower than in group n.2 (AUC $= 2.9 \pm 0.74$). AUC values provide direct information about the vascularization of the tissues, showing that the tumor tissues from experimental group n.2 ($2 * 10^6$ cells) are more vascularized. This is probably due to the larger average size reached by tumors in experimental group n.1, which is in line with the well-known feature of xenografts of being more vascularized at the tumor periphery [13].

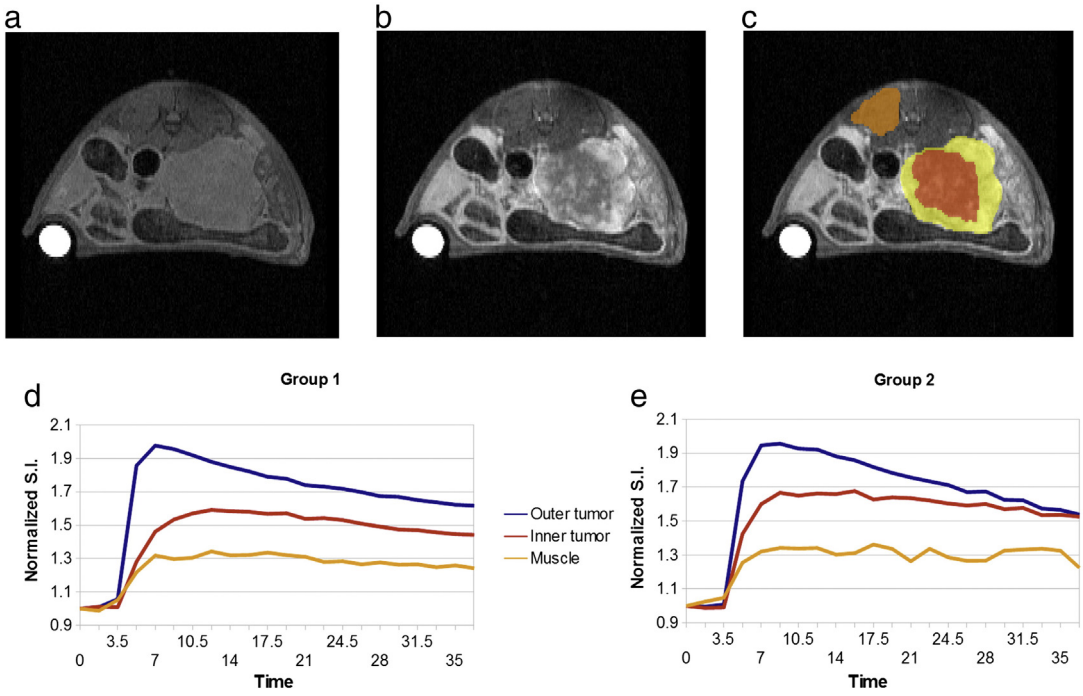

Fig. 2. DCE-MRI experiment: representative images and time course of the signal. a) T1 weighted image acquired in one animal belonging to experimental group n.1 before contrast agent injection. b) T1 weighted image acquired immediately after contrast agent injection. c) Image showing positioning of ROIs used to evaluate AUC in the external and internal part of the tumor and in the skeletal muscle. d) Time dependence of the signal intensity, normalized to pre contrast value, as a function of time (minutes) in the tumor periphery (outer tumor), in the tumor core (inner tumor) and in skeletal muscle (muscle) for one animal belonging to group n.1. e) Time dependence of the signal intensity for one animal belonging to the group n.2. The time course of the signal intensity for group n.2 clearly shows faster response to contrast agent in the core of the tumor when compared to group n.1. Outer tumor and muscle show similar behavior with respect to group n.1. The high intensity object in the lower left corner of images is a Gd-DTPA solution used as external standard to normalize the signal intensity during acquisition.

Please cite this article as: Ritelli R, et al, Pancreatic cancer growth using magnetic resonance and bioluminescence imaging, Magn Reson Imaging (2015), http://dx.doi.org/10.1016/j.mri.2015.02.017

3.5. MRI vs. BLI in a case of intestinal invasion

One mouse belonging to experimental group n.1 featured bowel tumor masses clearly detected by BLI but not by MRI. Images are shown in Fig. 3. One month after cell injection (Fig. 3a, on the left) weak bioluminescence was detectable both on the left and right sides of the abdomen. Two months after cell injection (Fig. 3a, on the right) several spots were detectable on the left side of the abdomen, in addition to the massive emission coming from the right part of the abdomen corresponding to the primary tumor. Fig. 3c and d shows coronal and transversal contiguous T2w MRI slices acquired two months after cell injection. While the primary tumor is clearly visible, no evidence of intestinal invasion is apparent. At necropsy the presence of small masses in the intestine (about 3 mm in diameters) was confirmed (see arrows in Fig. 3b). H&E staining confirmed that small masses excised from this subject were composed of tumor cells. The third month data are not available because the mouse had already been sacrificed.

3.6. Histology

After the third time point of acquisition all mice were sacrificed by cervical dislocation at the end of the last images data capture. During the necropsy, liver as well as the whole abdominal and thoracic cavities were carefully observed in order to detect potential tumor diffusion by macroscopic analysis. In a single animal, intestinal tumor masses were detected that indeed were also apparent in BLI acquisitions (see Fig. 3). After the first macroscopic analysis, primary tumors, spleen, residual normal pancreas and small intestine were excised for histology [14]. Fig. 4 reports macroscopic and histological images in representative animals. Fig. 4b shows H&E staining of a tumor mass excised from a mouse belonging to the group n.1 in which both imaging techniques revealed the tumor. H&E staining confirmed that the excised mass from this mouse was composed by tumor cells: the high number and morphological aspects of cells and the high degree of mitosis were important indicators of the tumor tissue. Moreover no evident signs of necrosis were detected. Fig. 4c shows the pancreas extracted from one animal belonging to the group n.2 in which neither MRI nor BLI detected tumor signal. In this case, H&E clearly shows normal pancreatic tissue.

In the lower line of Fig. 4 we report H&E staining of small masses collected from the small intestine of the only mouse that showed bowel tumor masses. H&E staining confirmed that these masses were tumor tissues.

4. Discussion

Reproducible preclinical models, as well as optimization of imaging techniques for monitoring tumor growth and metastasis formation, are crucial for the development of new and effective treatment modalities. Currently, several mouse models of pancreatic cancer have been established [15,5]. These include subcutaneously [16,17] and/or orthotopically [18,19] implanted xenografts of human

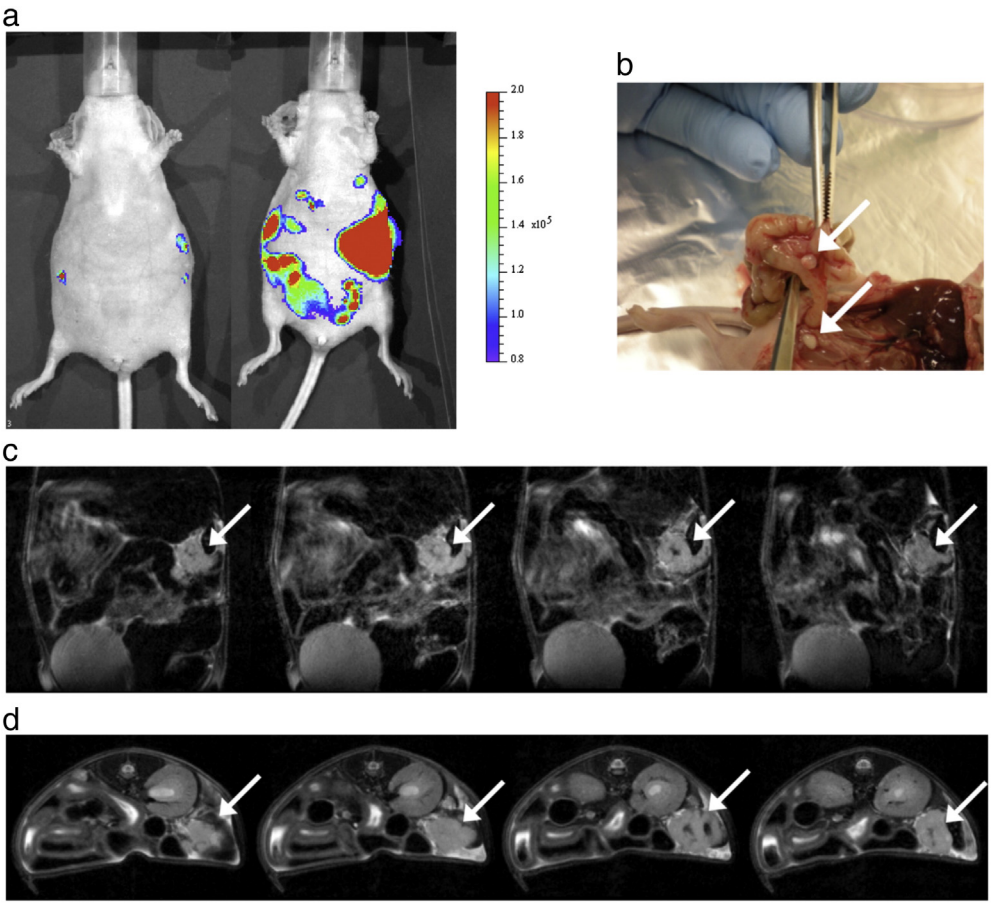

Fig. 3. Visualization of small bowel tumor masses. a) Optical Images acquired one (on the left) and two (on the right) months after cell injection. Color bar reports photon flux expressed as (number of photons)/s/cm2/sr.; b) macroscopic findings after sacrifice show small masses (arrows) in the small intestine; c) T2w MR images acquired in the coronal plane and d) in the axial plane show the clearly detectable primary tumor (indicated by arrows) but not bowel tumor masses.

Please cite this article as: Ritelli R, et al, Pancreatic cancer growth using magnetic resonance and bioluminescence imaging, Magn Reson Imaging (2015), http://dx.doi.org/10.1016/j.mri.2015.02.017

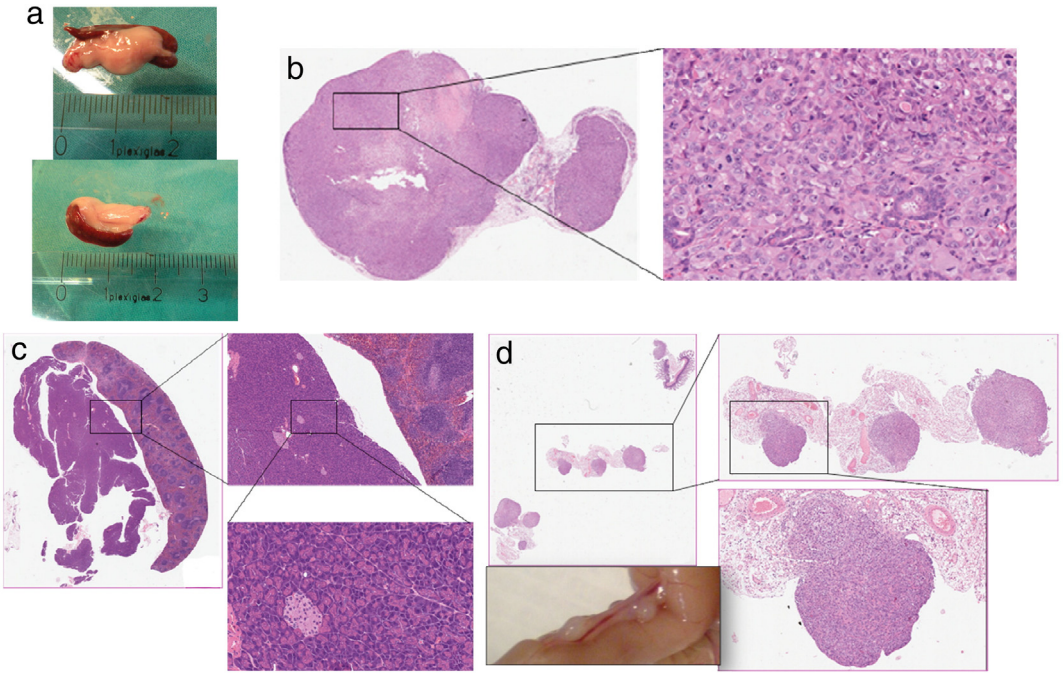

Fig. 4. Ex vivo and histological examinations. a) Photos of tumors excised from representative animals belonging to the group n.1. b) H&E staining of a tumor mass excised from a mouse belonging to the group n.1 in which both imaging techniques revealed the tumor. H&E staining confirmed that the excised mass from this mouse was composed by tumor cells. c) Pancreas and spleen extracted from one animal belonging to the group n.2 in which neither MRI nor BLI detected tumor signal. In this case, H&E clearly shows normal pancreatic tissue. d) H&E staining of masses collected from the small intestine of the only mouse that showed bowel tumor masses. H&E staining confirmed that these masses were tumor tissues.

tumor cells into SCID or nude mice as well as transgenic models [2]. In this study we focused on the behavior of Panc-1-Luc + cells when injected into the pancreas of nude mice. Because orthotopically implanted tumors grow deep within the abdomen, non-invasive imaging methods to assess their growth rate and potential dissemination over time are needed [12]. In this paper we used and compared optical imaging in the bioluminescence modality (BLI) with MRI.

First of all, we addressed the sensitivity of the two modalities. Two experimental groups were investigated in which tumors were induced by injecting $5 * 10^6$ and $2 * 10^6$ cells respectively. In the first group, as expected, tumors reached larger sizes and were detected with same sensitivity by both techniques. In the second group, characterized by smaller sizes, MRI proved less sensitive than BLI at the first time point. However MRI sensitivity increased up to 80% 3 months after injection.

Our results show that BLI is more sensitive than MRI in the case of the small tumors, and also in the detection of small bowel tumor masses where MRI failed. In fact one mouse displayed small light spots all over the abdomen while MRI only detected the main tumor mass (Fig. 3). At necropsy and histology, small masses were found throughout the bowel, which were confirmed to be tumor tissues.

In addition to sensitivity, a reliable in vivo imaging technique needs to meet the requirement of consistency of data. In the absence of therapeutic treatment, the tumor mass is expected to monotonically increase over time. This was observed in each subject using MRI, but not using BLI, which is a somewhat surprising finding. Simple T2w MRI cannot discriminate between viable and necrotic tumor tissue and one possible explanation for the above-mentioned finding could be the fact that, as MRI-detected tumor volume increases, the viable tumor mass detected by BLI may actually decrease. However we are inclined to exclude this possibility because histology did not indicate substantial necrotic areas, and also because this non-monotonic trend was mainly observed in experimental group n.2, characterized by tumors having smaller volumes and higher perfusion than those in group n.1. As mentioned before, photon attenuation from different depth of abdominal tissues could justify this finding. Other explanations for the observed signal attenuation in the middle time point could be the luciferin batch or scarce tumor perfusion, at this time point, that could partially prevent luciferin delivery to tumor cells. A similar non-monotonic trend of tumor BLI signal over time has been reported in one study of brain tumors [20]. In this study the authors used BLI and observed some animals with spontaneous regression of BLI signal but not of MRI volume. The authors stressed the potential confounding effect of similar subjects in any preclinical therapeutic response trials, and the value of using BLI and MRI in combination. Moreover other papers reported that the intensity of in vivo BLI signal strongly depends on the depth of the light source due to strong attenuation by overlying tissue [21].

In general, BLI signals have been found to correlate well with MRI measurements of tumor volumes (see Table 2). As far as experimental group n.1 is concerned, we can find a good correlation between MRI volumes and BLI photon fluxes, especially when we include in the analysis all acquisitions performed at the three time points. If we separately analyze all the data obtained 1, 2 and 3 months after cell inoculation, a good correlation is found only at the third time point. In experimental group n.2 the correlation between MRI and BLI was worst probably due to the smaller sizes of tumors corresponding to a smaller photon flux and also to a reduced number of animals. When BLI and MRI readouts were compared with ex vivo determined tumor volume, MRI was found to correlate better than BLI with ex-vivo values.

A poor correlation between BLI data and MRI/histology tumor volume has been reported in an experimental model of bladder cancer xenografts [22]. Interestingly, the correlation was poor in KU7

Please cite this article as: Ritelli R, et al, Pancreatic cancer growth using magnetic resonance and bioluminescence imaging, Magn Reson Imaging (2015), http://dx.doi.org/10.1016/j.mri.2015.02.017

xenografts, but good in 253JB-V xenografts. The second cell line produced tumors characterized by homogeneous distribution of vessels while the first produced tumors with necrotic core, vessels distributed in the tumor periphery [22] and hypoxic regions. These findings underline the importance of hypoxia and luciferin delivery to the tumor [22].

BLI is better than MRI when the aim is to detect small tumors, but shows problems of consistency as demonstrated by the non monotonic growth of the tumor photon fluxes as MRI-measured volumes increase. The variability of the tumor depth, leading to different absorption of photons, was probably the main cause of this erratic performance. On the other hand MRI shows a complementary pattern: it misses the smallest tumors but features great consistency over time and a monotonic trend with time elapsed after cell injection.

Moreover, DCE-MRI experiments could easily be conducted in this anatomical district. DCE-MRI provided us information about the vascularization of tumor masses, showing differences between the two groups of animals (tumors in group n.2 being more vascularized than in group n.1) and differences between external and internal regions of a given tumor. The external region was more vascularized than the internal one, which was in line with findings in other experimental models [13,23]. Moreover, since the enhancement of tumor tissue was higher than the enhancement of surrounding tissues, muscle and abdominal organs, it could help identification of tumor masses when the tumor is small.

Nowadays, luciferase transfected cell lines are extensively used for cancer models to assess in vivo growth, metastatic potential and response to therapies non-invasively by BLI. However, the possibility that luciferase-expression is associated with altered cell growth in vivo has been investigated in the literature with contradictory results [24]. In the present work this point has not been investigated because the focus was the comparison of two imaging modalities using a single cell line.

5. Conclusion

In conclusion, MRI and OI are two complementary techniques for in vivo imaging, both targeting crucial features of tumor development. In particular this study demonstrates that a bimodal approach combining MRI and BLI is necessary when developing an experimental platform for testing the efficacy of new therapeutic agents.

Acknowledgements

Supported by Italian Association for Cancer Research (A.I.R.C.) GRANT n.12182.

References

[1] Li D, Xie K, Wolff R, Abbruzzese JL. Pancreatic cancer. Lancet 2004;363(9414):1049–57.
[2] Herreros-Villanueva M, Hijona E, Cosme A, Bujanda L. Mouse models of pancreatic cancer. World J Gastroenterol 2012;18(12):1286–94.
[3] Marzola P, Sbarbati A. Magnetic resonance imaging in animal models of pathologies. Methods Enzymol 2004;386:177–200.
[4] Grassi R, Cavaliere C, Cozzolino S, Mansi L, Cirillo S, Tedeschi G, et al. Small animal imaging facility: new perspectives for the radiologist. Radiol Med 2009;114(1):152–67.
[5] Partecke IL, Kaeding A, Sendler M, Albers N, Kuhn JP, Speerforck S, et al. In vivo imaging of pancreatic tumours and liver metastases using 7 tesla MRI in a murine orthotopic pancreatic cancer model and a liver metastases model. BMC Cancer 2011;11:40–54.
[6] Abou-Elkacem L, Gremse F, Barth S, Hoffman RM, Kiessling F, Lederle W. Comparison of muCT, MRI and optical reflectance imaging for assessing the growth of GFP/RFP-expressing tumors. Anticancer Res 2011;31(9):2907–13.
[7] Bhattacharya A, Turowski SG, San Martin ID, Rajput A, Rustum YM, Hoffman RM, et al. Magnetic resonance and fluorescence-protein imaging of the anti-angiogenic and anti-tumor efficacy of selenium in an orthotopic model of human colon cancer. Anticancer Res 2011;31(2):387–93.
[8] Gaviraghi M, Tunici P, Valensin S, Rossi M, Giordano C, Magnoni L, et al. Pancreatic cancer spheres are more than just aggregates of stem marker-positive cells. Biosci Rep 2011;31(1):45–55.
[9] Sohn TA, Su GH, Ryu B, Yeo CJ, Kern SE. High-throughput drug screening of the DPC4 tumor-suppressor pathway in human pancreatic cancer cells. Ann Surg 2001;233(5):696–703.
[10] Marzola P, Degrassi A, Calderan L, Farace P, Nicolato E, Crescimanno C, et al. Early antiangiogenic activity of SU11248 evaluated in vivo by dynamic contrast-enhanced magnetic resonance imaging in an experimental model of colon carcinoma. Clin Cancer Res 2005;11(16):5827–32.
[11] Marzola P, Degrassi A, Calderan L, Farace P, Crescimanno C, Nicolato E, et al. In vivo assessment of antiangiogenic activity of SU6668 in an experimental colon carcinoma model. Clin Cancer Res 2004;10(2):739–50.
[12] Bouvet M, Spernyak J, Katz MH, Mazurchuk RV, Takimoto S, Bernacki R, et al. High correlation of whole-body red fluorescent protein imaging and magnetic resonance imaging on an orthotopic model of pancreatic cancer. Cancer Res 2005;65(21):9829–33.
[13] Boschi F, Marzola P, Sandri M, Nicolato E, Galie M, Fiorini S, et al. Tumor microvasculature observed using different contrast agents: a comparison between Gd-DTPA-albumin and B-22956/1 in an experimental model of mammary carcinoma. Magn Reson Mater Phys 2008;21(3):169–76.
[14] Ritelli R. Generating a pancreatic cancer mouse model: from cancer stem cells to in vivo imaging strategies. Dissertation University of Verona; 2010.
[15] Lehmann A, Denkert C, Budczies J, Buckendahl AC, Darb-Esfahani S, Noske A, et al. High class I HDAC activity and expression are associated with RelA/p65 activation in pancreatic cancer in vitro and in vivo. BMC Cancer 2009;9:395–405.
[16] Loos M, Hedderich DM, Ottenhausen M, Giese NA, Laschinger M, Esposito I, et al. Expression of the costimulatory molecule B7-H3 is associated with prolonged survival in human pancreatic cancer. BMC Cancer 2009;9:463–73.
[17] Peiper M, Nagoshi M, Patel D, Fletcher JA, Goegebuure PS, Eberlein TJ. Human pancreatic cancer cells (MPanc-96) recognized by autologous tumor-infiltrating lymphocytes after in vitro as well as in vivo tumor expansion. Int J Cancer 1997;71(6):993–9.
[18] Talmadge JE, Singh RK, Fidler IJ, Raz A. Murine models to evaluate novel and conventional therapeutic strategies for cancer. Am J Pathol 2007;170(3):793–804.
[19] Kalinina T, Gungor C, Thieltges S, Moller-Krull M, Penas EM, Wicklein D, et al. Establishment and characterization of a new human pancreatic adenocarcinoma cell line with high metastatic potential to the lung. BMC Cancer 2010;10:295–308.
[20] Jost SC, Collins L, Travers S, Piwnica-Worms D, Garbow JR. Measuring brain tumor growth: combined bioluminescence imaging–magnetic resonance imaging strategy. Mol Imaging 2009;8(5):245–53.
[21] Inoue Y, Izawa K, Tojo A, Nomura Y, Sekine R, Oyaizu N, et al. Monitoring of disease progression by bioluminescence imaging and magnetic resonance imaging in an animal model of hematologic malignancy. Exp Hematol 2007;35(3):407–15.
[22] Black PC, Shetty A, Brown GA, Esparza-Coss E, Metwalli AR, Agarwal PK, et al. Validating bladder cancer xenograft bioluminescence with magnetic resonance imaging: the significance of hypoxia and necrosis. BJU Int 2010;106(11):1799–804.
[23] Marzola P, Ramponi S, Nicolato E, Lovati E, Sandri M, Calderan L, et al. Effect of tamoxifen in an experimental model of breast tumor studied by dynamic contrast-enhanced magnetic resonance imaging and different contrast agents. Invest Radiol 2005;40(7):421–9.
[24] Johnson CH, Fisher TS, Hoang LT, Felding BH, Siuzdak G, O'Brien PJ. Luciferase does not alter metabolism in cancer cells. Metabolomics 2014;10(3):354–60.

Please cite this article as: Ritelli R, et al, Pancreatic cancer growth using magnetic resonance and bioluminescence imaging, Magn Reson Imaging (2015), http://dx.doi.org/10.1016/j.mri.2015.02.017